Polymer 55 (2014) 258–270

Contents lists available at ScienceDirect

Polymer

journal homepage: www.elsevier.com/locate/polymer

Nanocomposites from styrene-butadiene rubber (SBR) and multiwall carbon nanotubes (MWCNT) part 1: Morphology and rheology

S.K. Peddini [a], C.P. Bosnyak [b], N.M. Henderson [b], C.J. Ellison [a], D.R. Paul [a,*]

[a] Department of Chemical Engineering and Texas Materials Institute, The University of Texas at Austin, Austin, TX 78712, USA
[b] Molecular Rebar Design, LLC, 13477 Fitzhugh Rd, Austin, TX 78736, USA

ARTICLE INFO

Article history:
Received 16 July 2013
Received in revised form
30 October 2013
Accepted 1 November 2013
Available online 13 November 2013

Keywords:
MWCNT-SBR masterbatch
Rheology
Dilution

ABSTRACT

Because of the exceptionally high modulus and aspect ratios of multiwall carbon nanotubes (MWCNT), there has been much interest in using them as reinforcing agents for polymer composites. However, the commercial implementation of such nanocomposites has generally met with very limited success owing to poor dispersion of the MWCNT in the polymer matrix. A strategy that overcomes many of these difficulties is described here with a view towards incorporating MWCNT with carbon black or silica for improved elastomer performance in such applications as tires. Key issues are control of the MWCNT surface functionality for proper individual tube dispersion, their aspect ratio for a balance of mechanical performance versus melt processability and an appropriate masterbatch concentration for ease of further formulation by rubber goods manufacturers. Styrene-butadiene rubber (SBR), commonly used as a tread stock for tires, is employed here as the matrix for creation of a masterbatch with oxidized MWCNT (12.3–15 wt.%). Masterbatch rheology is necessary to understand how to achieve good dispersion and conformation of the MWCNT in the final product. Rheological characterization of the masterbatch nanocomposites and their dilutions over shear rate ranges relevant for processing will be described. Scanning transmission electron microscopy (STEM) investigations have revealed that this process produces good dispersion of the MWCNT's in the SBR matrix. The distribution of diameters, contour lengths, and end-to-end distances of the MWCNT in these formulations has also been determined. Effective tube aspect ratios for the nanocomposites with various MWCNT loadings were estimated by analysis of the rheological data for uncured specimens and the dynamic mechanical properties of cured composites using the Guth–Gold–Smallwood theory. These materials do not show a high level of electrical conductivity as might be expected from a percolation concept, signifying excellent tube dispersion and formation of a bound rubber layer on the discrete MWCNT.

© 2013 Elsevier Ltd. All rights reserved.

1. Introduction

Since the documented discovery of carbon nanotubes (CNTs) by Iijima [1] in 1991, polymer–CNT composite materials have been the subject of much academic and industrial research using different polymers including elastomers to improve mechanical and electrical properties [2–11]. CNTs can be classified by the number of walls in the tube, singlewall, doublewall and multiwall (MW), each wall can be further classified into chiral or non-chiral forms. Carbon nanotubes are generally manufactured commercially via a chemical vapor phase deposition process using iron, cobalt or nickel catalysts. The nanotubes usually exist as agglomerated balls or bundles, due to van der Waals attraction forces between them [12], as taken directly from the reactor and can contain significant amounts (5–25 wt.%) of residual catalysts and char. Based on the method of synthesis, CNTs exhibit very high aspect ratios, i.e., length to diameter ratio, up to 1000 [13], and also have a very high tensile modulus. As a result, carbon nanotubes are predicted to have significant utility as a reinforcing agent in polymer composites. However, commercial utilization of carbon nanotubes in these applications has been hampered by the general inability to reliably separate and disperse individualized carbon nanotubes in the polymer matrix. To reach the full potential of performance enhancement by carbon nanotubes in polymer composites, the aspect ratio should be substantially greater than 10, but not so high as to cause problems, such as high viscosity, that preclude processing. The maximum aspect ratio for a given tube length is reached when each tube is fully separated from others. A bundle of carbon nanotubes, for example, has an effective aspect ratio in composites of the order of the bundle length divided by its

* Corresponding author. Tel.: +1 512 471 5392; fax: +1 512 471 0542.
E-mail address: drp@che.utexas.edu (D.R. Paul).

0032-3861/$ – see front matter © 2013 Elsevier Ltd. All rights reserved.
http://dx.doi.org/10.1016/j.polymer.2013.11.003

LGES 1024

diameter. Carbon nanotubes can also have defects in the regular hexagonal lattice structure of the walls, particularly in the end-caps, that create curvature; these defects are considered to consist primarily of heptagon-pentagon structures [14]. Fig. 1 shows estimates of the enhancement in modulus and viscosity (ratio of composite to matrix value) as a function of aspect ratio for 10 wt.% CNTs in a natural rubber matrix calculated using the Halpin-Tsai model for composites and a rigid rod viscosity percolation model [15]. These calculations suggest that aspect ratios in the range of 50–100 represent a practical optimum for balancing mechanical performance and processability.

MWCNTs usually exist as bundles or agglomerates depending on the method of their synthesis. These agglomerates, also known as "primary aggregates", act as defects and must be avoided in order to improve the mechanical properties and processability of the composite material. Various methods have been developed to debundle or disentangle carbon nanotubes and, hence, to increase the effective aspect ratio in polymer matrices; these include chemical functionalization of the tube surfaces [16–18], in-situ emulsion polymerization [19–21], oxidation [22], sonication [16,23], coagulation [24], melt compounding [25–27], solution mixing [28], and use of surfactants [29]. Datsyuk et al. [30] have analyzed various oxidation techniques for MWCNTs and the primary products of oxidation are carboxylic acids, hydroxyl groups and lactones. Most of the aforementioned techniques have been used in dispersion of MWCNTs in thermoplastics, epoxies, and fibers to varying degrees of success, but very little research has been reported on enhancing the dispersion of oxidized MWCNTs in elastomers like styrene-butadiene rubber, (SBR) or targeting tire formulations. SBR is one of the important constituents in the current tire industry, and incorporation of MWCNTs can offer improvements in tear, crack resistance and other mechanical properties due to the reportedly high Young's modulus of the MWCNT (1–1.8 TPa) and tensile strength (~100 GPa) [31]. When MWCNTs are dispersed well (or debundled from their original "primary aggregates") in the polymer matrix, they form a continuous filler network at a threshold MWCNT loading, known as a "percolated network", beyond which point the properties, for example, viscosity, electrical conductivity, etc., exhibit a different response to the filler loading than below the percolation threshold. The percolation threshold is dependent on the aspect ratio of the tubes and their degree of dispersion [32]. Of note, if the tubes are not straight, then one has to consider an "effective aspect ratio" which may be considered as the ratio of the persistence length of the tube in a given direction to the tube diameter.

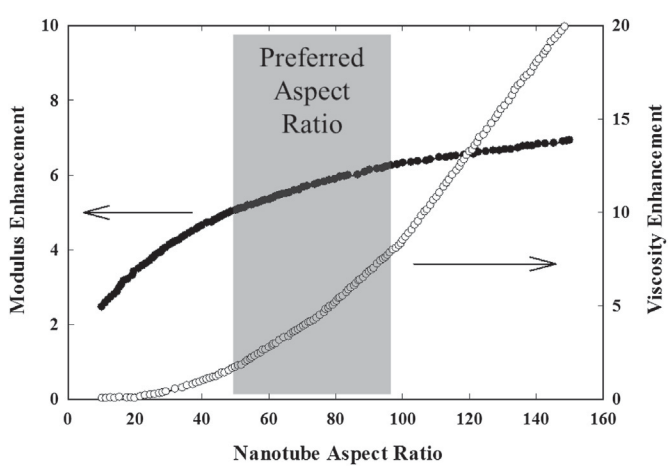

Fig. 1. Calculated modulus and viscosity enhancements of composites containing 10 wt.% MWCNT in a natural rubber matrix as a function of MWCNT aspect ratio.

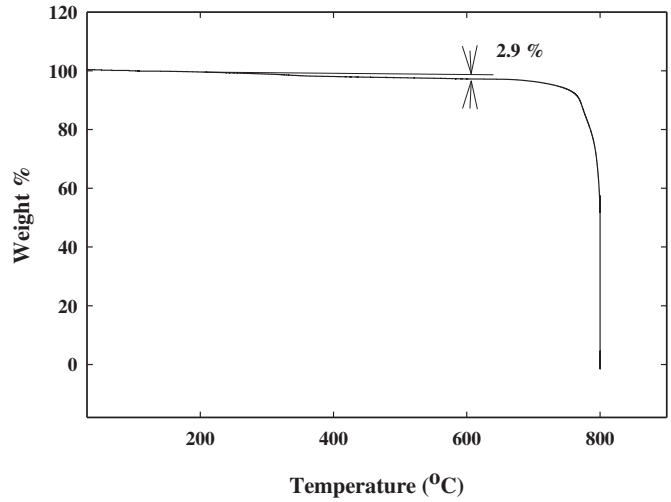

Fig. 2. Thermogravimetric analysis of oxidized MWCNTs.

The global tire industry was valued at $131.5 billion in 2011 [33] with a continuous growth of 1.1% per year from 2006 to 10. To effectively and economically take advantage of any use of MWCNTs in the tire formulations, manufacturers need the freedom of diluting a preformed MWCNT-rubber masterbatch and the ability to blend the masterbatch with different rubbers to produce tires for different climatic conditions. For example, SBR is a main component in tires in the Southern US compared to natural rubber as a main component in tires in Canada. This requires a good understanding of the MWCNT dispersion, effective aspect ratio, viscosity and mechanical properties of the diluted compositions in comparison with the original masterbatch in order to design high performance products. Abdel-Goad and Pötschke [34–37] have studied the dilution of polycarbonate-MWCNT masterbatches to understand the dispersion of MWCNTs, electrical conductivity and effects of tube aggregation with mixing time, shear rate and viscosity of the matrix. Their work illustrated that MWCNT's can aggregate to form connected networks when the surface thermodynamics of the tube is not well-matched to that of the matrix. In this study, the thermodynamics of the tube surfaces and matrix are better balanced to avoid re-aggregation of the MWCNTs. The work presented here aims to provide an understanding of the viscosity of the surface modified MWCNT-SBR masterbatches and the dispersion of the MWCNTs at different mixing temperatures and mixing times. A further aim is to dilute these masterbatches with SBR to understand how the dispersion of MWCNTs in the matrix, the effective aspect ratio, the viscosity and electrical properties change. Both studies will serve to guide the design of masterbatches (by the producer) and its dilution into the same host rubber matrix or blending with a different rubber (by the user) to control the final dispersion of the surface modified MWCNTs, viscosity and mechanical properties. A lab-scale batch mixer was used in this work to study the rheology of these mixtures because of its similar mixing profile to industrial scale Banbury batch mixers. The batch mixer also provides a convenient way to track changes in the morphology with dilution of the MWCNT content. Future work will focus on the mechanical properties of the cured composites of the diluted and original masterbatches and failure mechanisms of the MWCNT-rubber composites. Subsequent studies with a MWCNT masterbatch will address selective filler interactions in blends of different rubbers (for example, natural rubber or butyl rubber with SBR) containing other fillers like silica and carbon black, etc.

2. Experimental

2.1. Materials

The oxidized multiwall carbon nanotubes used here, commercially known as Molecular Rebar™, were supplied by Molecular Rebar Design LLC. The multiwall carbon nanotubes consist of about 10–12 walls with an average outer wall diameter of 13 nm and a length range of about 200–1400 nm. The tubes have an overall oxidation level of 2.9 wt.% as determined by a TA instruments Q 50 thermogravimetric analyzer, TGA. The procedure for TGA analysis is to determine the weight loss in a nitrogen atmosphere over the temperature range of 200–600 °C, as shown in Fig. 2. At 700 °C, the atmosphere was switched to oxygen to burn off the carbon so as to determine the percent residual metals from the catalysts found to be 0.6 wt.%. Considering the oxidation is at the ends and outer and inner wall only, this overall oxidation level translates to an outer wall surface functionalization of about 10 wt.%. The oxidized species consist of approximately equimolar concentrations of carboxylic acid, hydroxyl and ketone groups as determined by XPS and subsequent analysis of the O1s binding states. From now onwards, these oxidized multiwall carbon nanotubes used in this work are designated as MWCNTs for convenience.

The presence of the carboxylic acid group on the tubes is demonstrated by the infra-red spectral peak around 1715 cm^{-1} using a KBr disk on a Bruker Alpha-P FTIR spectrometer, as shown in Fig. 3.

Oxidized MWCNTs taken from the filter cake following filtering and washing steps were examined by scanning electron microscopy (SEM). From the SEM micrograph in Fig. 4a, it can be seen that the tubes are open at the ends. The diameter distribution resulting from an analysis of 20 tubes is shown in Fig. 4b.

The contour lengths (see the microscopy section) of the tubes were also estimated from SEM images (see Fig. 5) obtained as follows. A dilute solution (1×10^{-6} g/ml) of separated carbon nanotubes was made in water containing the surfactant sodium dodecyl sulfate. A drop of the dilute solution was placed on carbon tape and dried. The tube lengths were determined using ImageJ software (as described in microscopy section) and the average length of the separated carbon nanotubes was found to be 500 nm. It is interesting to see in the micrograph (Fig. 5a) the presence of micelles of the surfactant uniformly distributed on the tube surface. Fig. 5b shows the distribution of tube lengths.

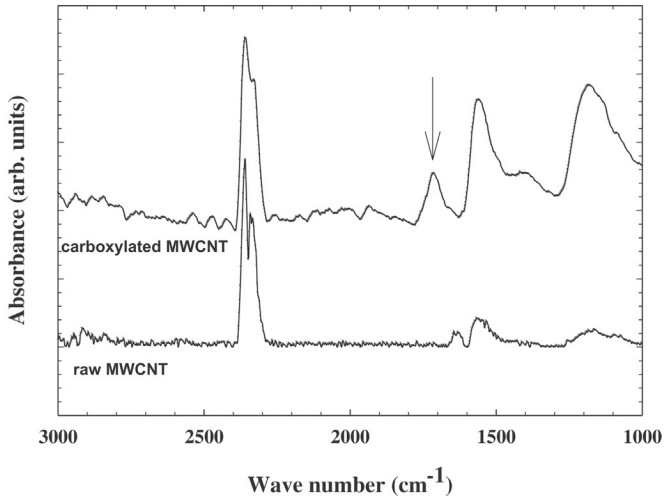

Fig. 3. Infra-red spectra of oxidized MWCNTs in comparison with unmodified MWCNT showing peaks at 1715 cm^{-1} related to –COOH groups.

Emulsion SBR 1502 latex was obtained from Styron LLC with a solid content of 25 wt.%. The polymer is stated to have 23.5% styrene content and a Mooney viscosity of 50 (ML 1 + 4 (100 °C)). The antioxidant used here is N-(1, 3-dimethylbutyl)-N′-phenyl-p-phenylenediamine, commonly termed 6PPD.

2.2. Masterbatch and unfilled SBR matrix preparation

Masterbatches of the oxidized MWCNT with styrene-butadiene rubber (SBR) were prepared using two methods, one by coagulation with acetone and the other by an aqueous coagulation method followed by mastication in a twin screw extruder.

2.2.1. Acetone coagulation

A masterbatch (MB) containing 15% by wt. of MWCNT was prepared by first dispersing the oxidized MWCNTs to a concentration of 1 wt.% in water using sodium dodecylbenzenesulfonate (SDBS) (Aldrich) to aid dispersion in a high intensity mixer; the mass ratio of SDBS to dry MWCNT was 1.5. This mixture was then added to the SBR 1502 latex in the ratio to give 15 wt.% MWCNT based on SBR. Acetone was added slowly while stirring the dispersion of MWCNT and latex to coagulate the rubber-MWCNT concentrate, that was then filtered from the effluent. The coagulated SBR-MWCNT masterbatch was cut into small pieces and dried at 45 °C for at least 48 h to remove any water and acetone. A control SBR sample was prepared by the same process, but with no surfactant or MWCNT added.

2.2.2. Aqueous coagulation/melt mastication

A second masterbatch with 12.3 wt.% MWCNT was made as above except the coagulation was performed using a high shear mixer. A microtome slice of a typical coagulated particle of the masterbatch is shown in Fig. 6. The SBR is seen as agglomerated domains of about 0.4–1.2 micron in diameter surrounded by a concentrated shell of carbon nanotubes.

2.3. Rheology of 15 wt.% MWCNT-SBR masterbatch (MB)

Rheological measurements of the MWCNT-SBR masterbatches were made at 140, 150 and 160 °C to obtain viscosity, η, as a function of shear rate, $\dot{\gamma}$, using a Haake Rheomix batch mixer with a roller-rotor mixing configuration. Temperatures between 140 and 160 °C were chosen to replicate industrial mixing conditions. To obtain consistent data, the ratio of the volume of the polymer to the mixer cavity volume with the roller-rotors, or fill factor, was set to 67%. The fill factor was calculated by considering the density of the SBR (0.94 g/cm^3) and the density of the CNTs (1.85 g/cm^3). Masterbatches were manually cut into small pieces and dried under vacuum at 45 °C for at least 48 h to remove any moisture and solvent. Three different pre-weighed quantities (calculated based on the 67% fill factor for the batch mixer) of masterbatch were used for each rheological measurement at different temperatures. For example, for the rheological measurement at 140 °C, a measured quantity of masterbatch was studied by starting the mixer RPM at 10 min^{-1} and going up to 80 min^{-1}; at the end of the experiment, the post-mixed material was taken out, labeled and kept aside. The same procedure was used for 150 and 160 °C measurements with a fresh sample used for the same experimental shear rate range to eliminate any effect of thermal degradation and shear history on the samples.

Our initial rheology measurements on a masterbatch without any antioxidant yielded cross-linked material at the end of the scans for all three temperatures (140, 150, and 160 °C). As a result, 2 phr (parts per hundred rubber) of 6PPD was used as an antioxidant for all rheological experiments reported here. A typical

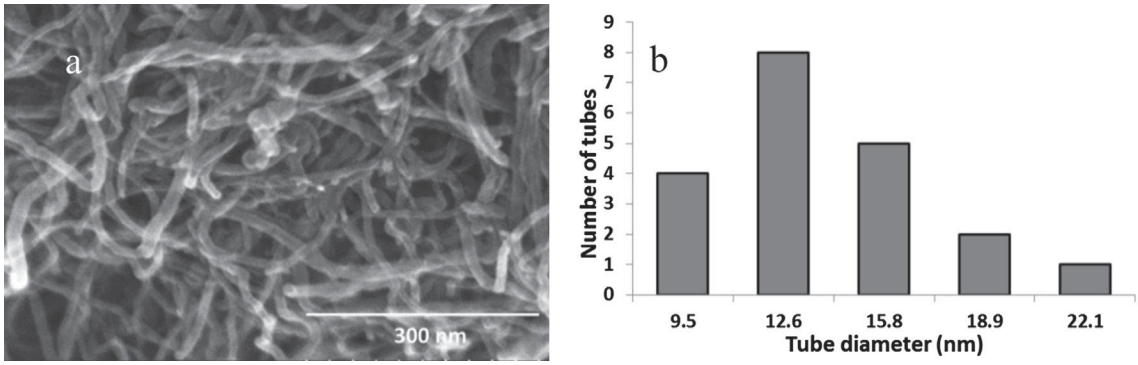

Fig. 4. a) Scanning electron micrograph for oxidized MWCNTs showing open-ended tubes. b) Diameter distribution of 20 tubes obtained from this image.

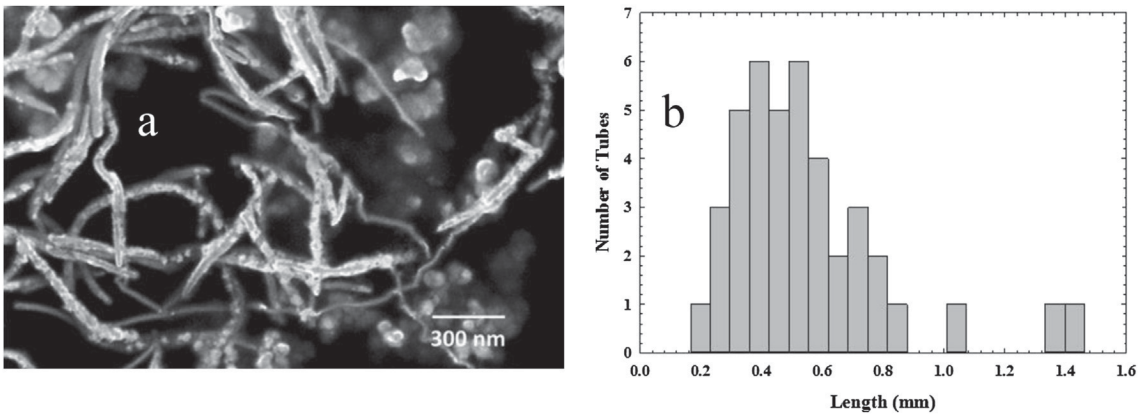

Fig. 5. a) Scanning electron micrograph for oxidized MWCNTs dispersed with sodium dodecyl sulfate (SDS) in water, b) length distribution of tubes calculated from micrographs such as Fig. 5a.

sampling of data for a masterbatch at 140 °C for two steps of RPMs is shown in Fig. 7. Fig. 7a shows the RPM increments, Fig. 7b shows the changes in temperature resulting from the changes in RPM, and Fig. 7c shows the torque versus time. In Fig. 7c, the dashed lines indicate the average torque value when the temperature reached 140 ± 0.5 °C.

One important point to consider in these rheological experiments is the length of time for each shear rate scan. The presence of 15 wt.% MWCNTs in the SBR matrix causes a considerable amount of viscous (frictional) heating during mixing; thus, bringing the temperature to the desired level via air cooling especially at high RPM (shear rate) took considerable time. A complete scan over the desired RPM or shear rate range, 10–80 min^{-1} (shear rate), took 265 min at 140 °C, 146 min at 150 °C and 97 min at 160 °C.

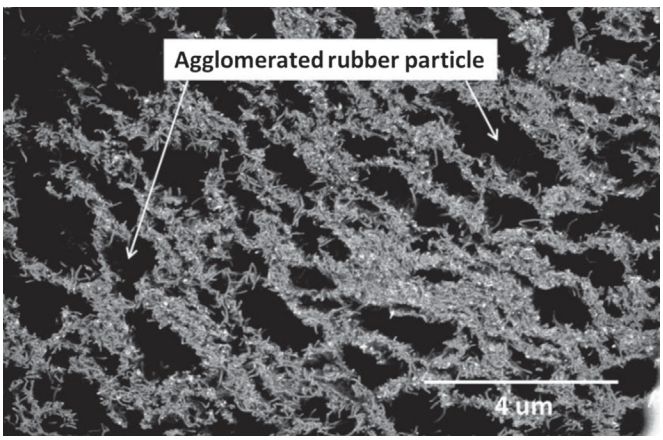

Fig. 6. SEM image of coagulated MWCNT-SBR masterbatch showing agglomerated SBR particles surrounded by MWCNTs.

2.4. Dilution of masterbatch with SBR

The 12.3 wt.% MWCNT-SBR masterbatch was used for dilution studies by adding calculated amounts of coagulated SBR 1502 rubber to prepare composites containing 1, 2, 3, 4, 5, 7.5 and 10 wt.% MWCNT using the Haake batch mixer. As mentioned, 6PPD was used as an antioxidant (A/O) to prepare these diluted masterbatches to prevent the oxidative cross-linking of the rubber. Initially, all three components (masterbatch, SBR and 2 phr 6PPD) were mixed in a small container and roughly half the amount of this mixture was added to the pre-heated Haake Batch mixer at 125 °C with screws rotating at 10 RPM. Once the mixture started fluxing, the speed was increased to 20 RPM and the remaining material was added, finally the feeder was closed with a 5 kg weight. Mixing was performed for a further 10 min after the temperature reached 140 °C. The dilution procedure involved total time of mixing from the beginning to the end of approximately 30 min.

2.5. Microtoming/scanning transmission electron microscopy (STEM)

Ultra-thin sections of ~50–60 nm were cut cryogenically from various composites containing antioxidants with a diamond knife

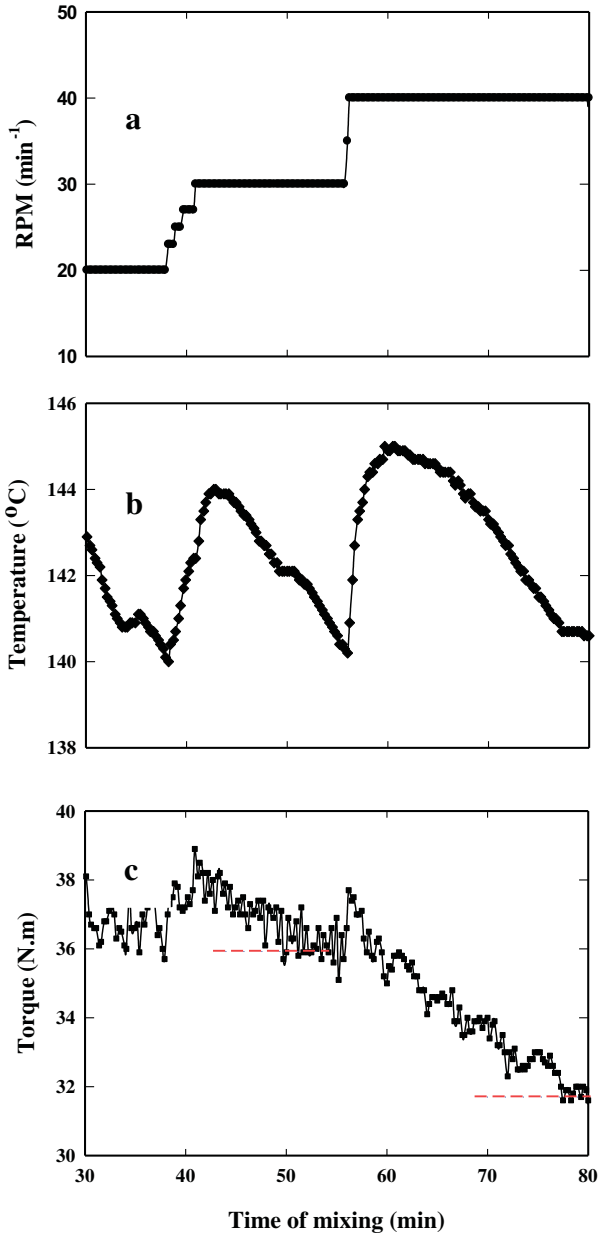

Fig. 7. Changes in a) RPM, b) temperature and c) torque for a masterbatch containing 15 wt.% MWCNT as a function of time of mixing.

maintained at −65 °C and a specimen temperature of −75 °C using an RMC PowerTome XL ultramicrotome. Dispersion of MWCNTs in the SBR matrix was observed by using a Hitachi S-5500 Scanning Electron Microscope (SEM) in bright field transmission (BF-STEM) mode at an accelerating voltage of 30 kV.

2.6. Curing procedure

The original masterbatch (12.3 wt.% MWCNT) and all of the diluted composites were mixed with curing agents in the Haake batch mixer in two stages. In stage 1, measured amounts of masterbatch (43 g), zinc oxide (2 g), stearic acid (1 g), and 6PPD (1 g) were mixed at 140 °C at a speed of 75 RPM for 10 min. The mixer was stopped and material was taken from the chamber while it cooled to about 75 °C for stage 2. Post-stage 1 material (MB, ZnO, SA, and 6PPD mixture) was mixed with crosslinker, S (0.5 g), and an accelerator ((N-tertiarybutyl-2-benzothiazole sulfonamide) (TBBS, 0.5 g)) first at 20 RPM and then rotor speed was slowly increased to 50 RPM. In stage 2 of mixing, the temperature was not allowed to go beyond 95 °C to prevent any onset of thermal crosslinking, while mixing was continued for 2 min. Post-stage 2 material was cooled to room temperature and cut into smaller pieces and pressed on a Wabash hot press at 160 °C and 45 ton in a 1.9 mm × 152.4 mm × 152.4 mm film mold for 20 min of heating and 2 min of air-cooling. All characterization measurements for these samples were performed 24 h after this curing step.

2.7. Electrical resistivity measurements

An Agilent 4362B LCR meter was used together with a custom-made test unit to measure electrical resistivity. The test unit consists of a PVC threaded pipe with a $^{3}/_{4}$ inch (19.05 mm) inside diameter through which a brass cylinder of length 3 inches (76.2 mm) and diameter 18.66 mm can slide. One end of the brass cylinder has a copper tab soldered onto it. The other end of the test device is a threaded plastic pipe of height 16 mm with a copper plate attached with superglue.

The machine thread of the clamp was calibrated in terms of distance versus number of turns, 4.2 mm/full turn. The LCR meter open circuit measurement was first performed according to the instrument manual. Samples of measured dimensions (length, width and thickness) were cut from uncured composites pressed at 100 °C in a Carver press at 5 ton for 2 min. The specimen was then placed in the test unit and a constant pressure (20 psi) was applied for each and every measurement. Each specimen was loaded such that at the end of 5 min the pressure was 20 psi and then the resistance measurements, R, were made. A frequency of 1000 Hz was used throughout with 0 V DC bias. The application of 20 psi pressure on a 1.92 mm thick 1 wt.% MWCNT composite resulted in a thickness reduction by 0.5 mm at a Shore A hardness value of 50. The thickness reduction was estimated for samples of increasing hardness (with increase in wt.% of MWCNT in the composite) by taking 0.5 mm and normalizing it by the Shore A hardness of the specimen divided by 50. The bulk resistivity, R_b, is given by

$$R_b = R\frac{A}{t} \tag{1}$$

where, A and t are the area and thickness after correction for the sample, respectively.

2.8. Viscosity calculations for Haake batch mixer

Conventional parallel plate rheometry was used initially to study the rheology of these composite materials, but due to slippage between the plates, a Haake batch mixer was used instead. Another advantage of using a batch mixer is its similarity to the flow pattern expected for an industrial Banbury mixer. For most batch mixers, the output data are torque (Γ) vs. time (t) at the applied RPM (N). In order to study the rheology of these nanocomposites, the torque vs. time data must be converted into viscosity (η) vs. shear rate ($\dot{\gamma}$). The dimensions of the cavity, roller-rotor configuration and the gap are important parameters in determining the viscosity vs. shear rate values calculated from torque vs. RPM data. Porter and Goodrich [38] and Bousmina et al. [39] have suggested that the effective hydrodynamic radius; R_i (as shown in the schematic diagram Fig. 8), depends on the geometry of the cavity and gear ratio but is independent of the viscosity of the fluid under mixing conditions. R_i is an imaginary radius at which all shear mixing occurs and its value lies between the external radius of the cavity (R_e) and the distance between the axis of the rotor and

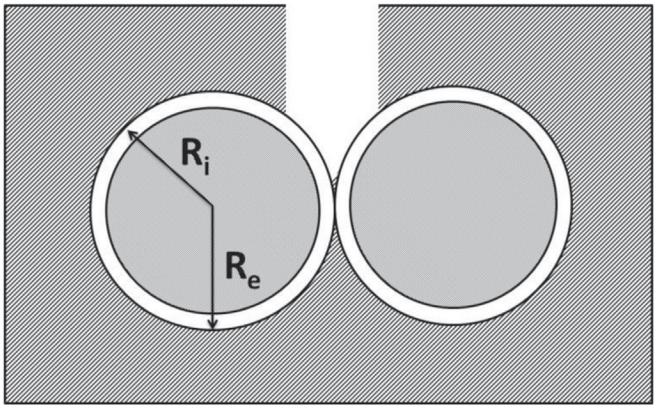

Fig. 8. Schematic representation of Haake batch mixer showing hydrodynamic radius (R_i) and external radius of the cavity (R_e).

it's tip. In the following we make use of the approach described by Bousmina et al. to calculate the effective hydrodynamic radius R_i for the Haake batch mixer by using polystyrene (PS685D obtained from Styron Chemicals) to correlate with rheological data obtained at the same temperature using cone-and-plate and capillary rheometers [40].

From the steady state torque (Γ) values for PS685D at 210 °C at the respective RPMs (N), viscosity (η) and shear rate ($\dot{\gamma}$) are calculated by using equations (2)–(5).

$$\eta = \frac{\Gamma}{N}\frac{\left(\beta^2 - 1\right)}{8\pi^2 L R_e^2 \left(1 + g^2\right)} \tag{2}$$

$$\beta = \frac{R_e}{R_i} \tag{3}$$

$$R_i = \frac{R_e}{\left[1 + \frac{4\pi N}{n}\left(2\pi M L R_e^2 \frac{1+g^{n+1}}{\Gamma}\right)^{1/n}\right]^{n/2}} \tag{4}$$

$$\dot{\gamma} = \frac{2\pi N}{\ln(\beta)} \tag{5}$$

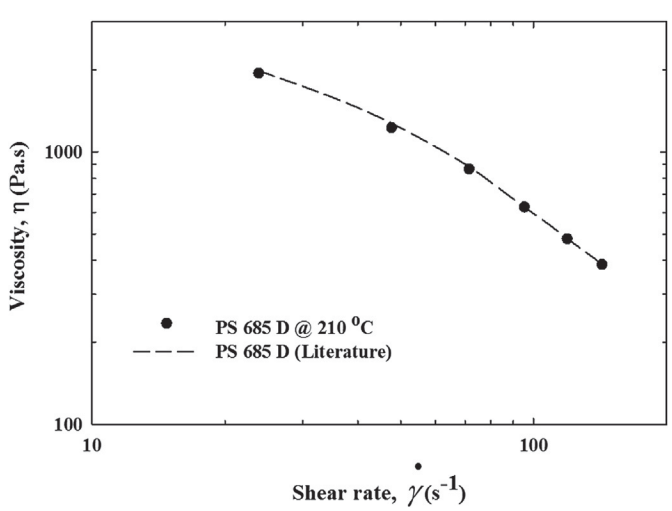

Fig. 9. Comparison of rheological data obtained for PS685D on a Haake mixer using a rotor-roller configuration at 210 °C with rheological data obtained for the same polymer from literature.

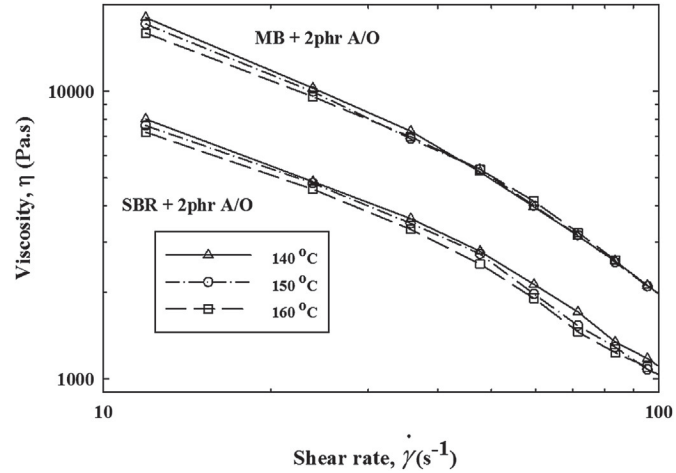

Fig. 10. Rheological behavior of SBR and MB measured in presence of 2 phr antioxidant (A/O) at 140, 150 and 160 °C, respectively, in the experimental shear rate range.

where N = RPM (s^{-1}), Γ = torque (N.m), R_e = external radius of the cavity (0.0196 m), R_i = hydrodynamic radius (0.0178 m), g = gear ratio of Haake mixer (here g = 2/3), L = length of the rotors (0.0466 m). M and n are power law parameters for PS685D at 210 °C, where, M, the consistency index (15,445 Pa.s^n) and n, power law index (0.277) following the power law relationship, $\eta = M\dot{\gamma}^{n-1}$. Comparison of the rheological data via the Haake batch mixer with the data obtained using other rheological measurements (cone-and-plate and capillary rheometers) on PS685D at 210 °C differs by only 0.5% over the measured shear rate range as shown Fig. 9. This comparison indicates the agreement between the two measuring techniques is excellent and validates the use of the Haake batch mixer as an alternative rheological instrument.

3. Results and discussion

3.1. Rheology of 15 wt.% MWCNT-SBR masterbatch

Fig. 10 shows the rheological behavior for a masterbatch (MB) containing 15 wt.% MWCNT (top curves) and the neat SBR 1502 (lower curves) samples measured at 140, 150 and 160 °C; a fresh

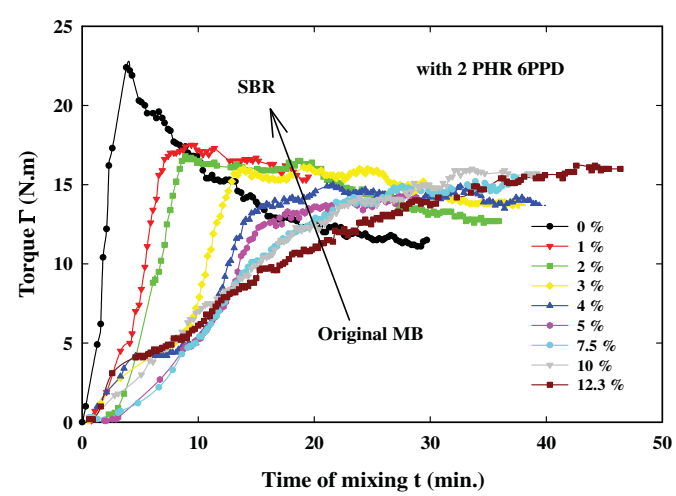

Fig. 11. Evolution of torque versus mixing time for 12.3 wt.% MWCNT-SBR masterbatch and various dilutions by adding SBR. (Note: For convenience, the control SBR sample with no surfactant or MWCNT was prepared by the process described in the experimental section and is labeled as 0%.).

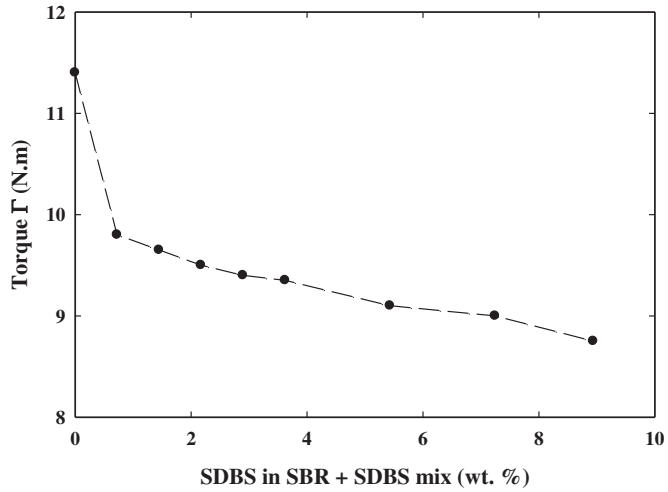

Fig. 12. Effect of SDBS on SBR torque at 140 °C and 20 RPM. (wt.% SDBS based on the total weight of SBR and SDBS).

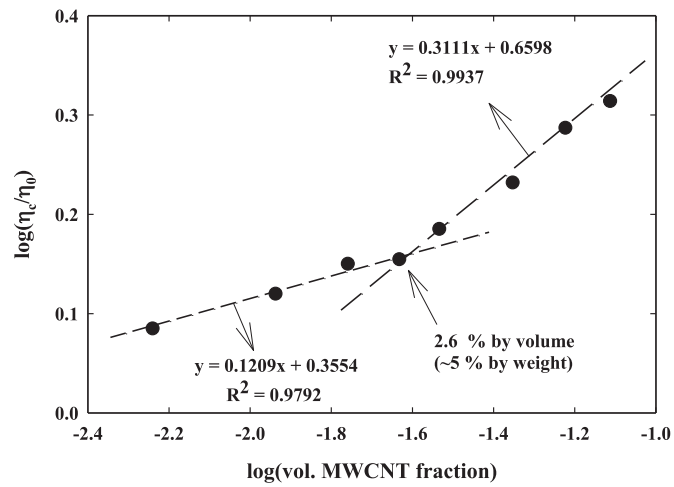

Fig. 14. Relative viscosity of nanocomposites vs. volume fraction of MWCNT to illustrate destruction of network of clusters in the original MB (12.3 wt.% MWCNT-SBR composite) with dilution.

sample was used for each temperature. Both the masterbatch and the SBR 1502 samples contain 2 phr 6PPD as an antioxidant. The rheological responses for the SBR 1502 matrix with antioxidant measured between 11.9 s^{-1} to 95.3 s^{-1} show that viscosity decreases with increasing temperature, increasing shear rate, or shear thinning, as expected for polymer fluids.

Surprisingly, the viscosity of the masterbatch is only about twice that of the SBR matrix at a given shear rate and temperature, and the rheological effects of changing shear rate and temperature are similar to that of neat SBR. The presence of antioxidant allows for lengthy experimental durations to minimize polymer degradation.

3.2. Dilution studies of 12.3 wt.% masterbatch

Fig. 11 shows the torque vs. mixing time for all the nanocomposites prepared by diluting the 12.3 wt.% MWCNT-SBR masterbatch to 1, 2, 3, 4, 5, 7.5 and 10 wt.% MWCNT by adding calculated amounts of SBR with 2 phr antioxidant 6PPD, to the Haake batch mixer at 140 °C at 20 RPM. For convenience, the control SBR sample with no surfactant or MWCNT was prepared by the process described in the experimental section and is labeled as 0%. The arrow indicates the direction of dilution. For the formulations rich in MWCNT, the torque shows a steady monotonic rise with mixing time to a final steady-state value. For pure SBR and formulations with low levels of MWCNT, the torque initially spikes to a maximum and then decreases to a final steady-state value. This response pattern is due to several factors including the slower heat transfer and lower stresses applied to the bulk of SBR pieces (~1 cubic cm) and relatively smaller original particle size (~0.1 cubic cm) of the masterbatch feed to the mixer. As the time of mixing increases, the torque value for the low MWCNT masterbatches decrease and reach a steady value. The initial spike in the torque decreases as more SBR is added to the original masterbatch and finally the spike disappears at 4 wt.% MWCNT and lower concentrations. The average torque value from the last 10 min of mixing used to calculate the viscosity of the composite discussed in the next section.

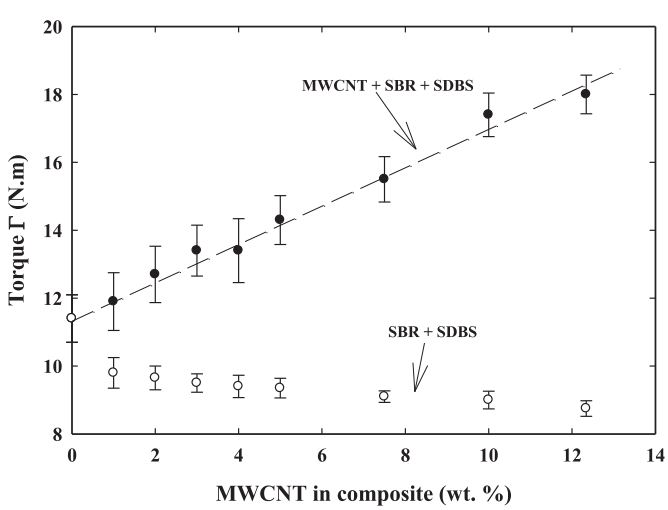

Fig. 13. Comparison of torque values of SBR containing the amount of SDBS in the diluted masterbatches determined as described in text.

From equation (2) in the previous section, the viscosity of each mixture can be computed for each operating RPM and temperature. In addition, the relative viscosity for each mixture can be calculated by dividing its measured torque at steady-state by the corresponding torque for SBR (matrix) at the same RPM and temperature. However, in the preparation of the masterbatches containing 12.3 wt.% MWCNT, SDBS was used as a surfactant in the following ratio SDBS: MWCNT in 1.5: 1 by weight and some surfactant remains in the mixture after coagulation which needs to be accounted for in computing the relative viscosity. The amount of surfactant retained in the masterbatch was determined by elemental analysis for sodium and sulfur. Torque values for SBR, at 140 °C and 20 RPM, containing equivalent amounts of SDBS present in the diluted composites are shown in Fig. 12.

The bottom curve (open circles) in Fig. 13 represents the torque values from Fig. 12 for SBR with the amounts of SDBS computed to be in each composite for a given wt.% MWCNT. The top curve in Fig. 13 (closed circles) represents the torque values for the diluted composite versus the amount of MWCNT contained. Fig. 13 shows representative error bars for both the composites and the SBR measurements.

From these results we see that the viscosity of the masterbatch containing 12.3 wt.% MWCNT is twice that of the matrix, including the effect of SDBS and antioxidant, at 140 °C and 20 RPM (23.8 s^{-1}). The viscosity of the composites relative to that of the matrix, with allowances for the surfactant amount as explained above, plotted

Table 1
Calculated aspect ratios from rheology measurements using Guth–Gold–Smallwood equation.

Relative viscosity η_c/η_0	Vol. MWCNT fraction, Φ	Calculated aspect ratio, α
1	0	–
1.21	0.006	36.6
1.32	0.012	24.2
1.41	0.017	19.3
1.43	0.023	14.8
1.53	0.029	13.7
1.70	0.045	10.9
1.93	0.060	9.7
2.06	0.077	8.1

versus vol.% of MWCNT loading calculated from wt.% MWCNT loading is shown in Fig. 14 on a log–log scale.

This plot appears to show two regimes with a change of slope about 2.5 X at 2.6 vol.%. It is believed that this change in slope may be a threshold composition for MWCNT delineating a change in how the MWCNT disperses in the SBR matrix. In the original concentrated masterbatch, the MWCNT exist as clusters and this continues as it is diluted with more SBR and the relative viscosity decreases along the upper branch of the log–log relation; however, below ~2.6 vol.% MWCNT, the relative viscosity is higher than expected based on an extrapolation of the upper branch, that is, the MWCNT enhances the viscosity more significantly, perhaps because the MWCNT disperse from the original clusters more nearly as independent nanotubes. Alternatively, this change in the MWCNT percolation network at ~2.6 vol.% with increase in MWCNT loading is analogous to formation of entanglements in polymer chain networks as seen with increase in molecular weight in polymer melts and concentrated solutions.

Another conventional method for analysis of the relative viscosity results is via the Guth–Gold–Smallwood equation [41–43]. This model assumes fillers are anisotropic and rigid with low aspect ratio. The effective aspect ratio α of the filler (MWCNT) can be calculated with the viscosity of the composite, η_c, volume fraction of MWCNT, Φ, and viscosity of the polymer matrix (SBR), η_0 as shown in equation (6).

$$\eta_c = \eta_0\left(1 + 0.67\alpha\Phi + 1.62\alpha^2\Phi^2\right) \tag{6}$$

The values of the aspect ratio calculated from the data via equation (6) for each volume fraction of MWCNT are shown in Table 1. The calculated aspect ratio increases as the concentration of MWCNT decreases. The calculated aspect ratios from the rheology measurements are lower than those determined by measuring them directly from TEM images due to the fact the tubes are not rigid rods but are flexible in the stress fields of rubber during mixing.

3.3. Morphology of the masterbatches containing 15 wt.% MWCNT after rheological mixing

Fig. 15 shows a collection of bright field scanning tunneling electron microscope (BF-STEM) images of microtomed cross-sections from the masterbatch containing 15 wt.% MWCNT. Fig. 15a shows an image of the masterbatch as prepared while Fig. 15(b–d) is images of this material after the rheological measurements at 140, 150 and 160 °C, respectively. Fig. 15a shows the

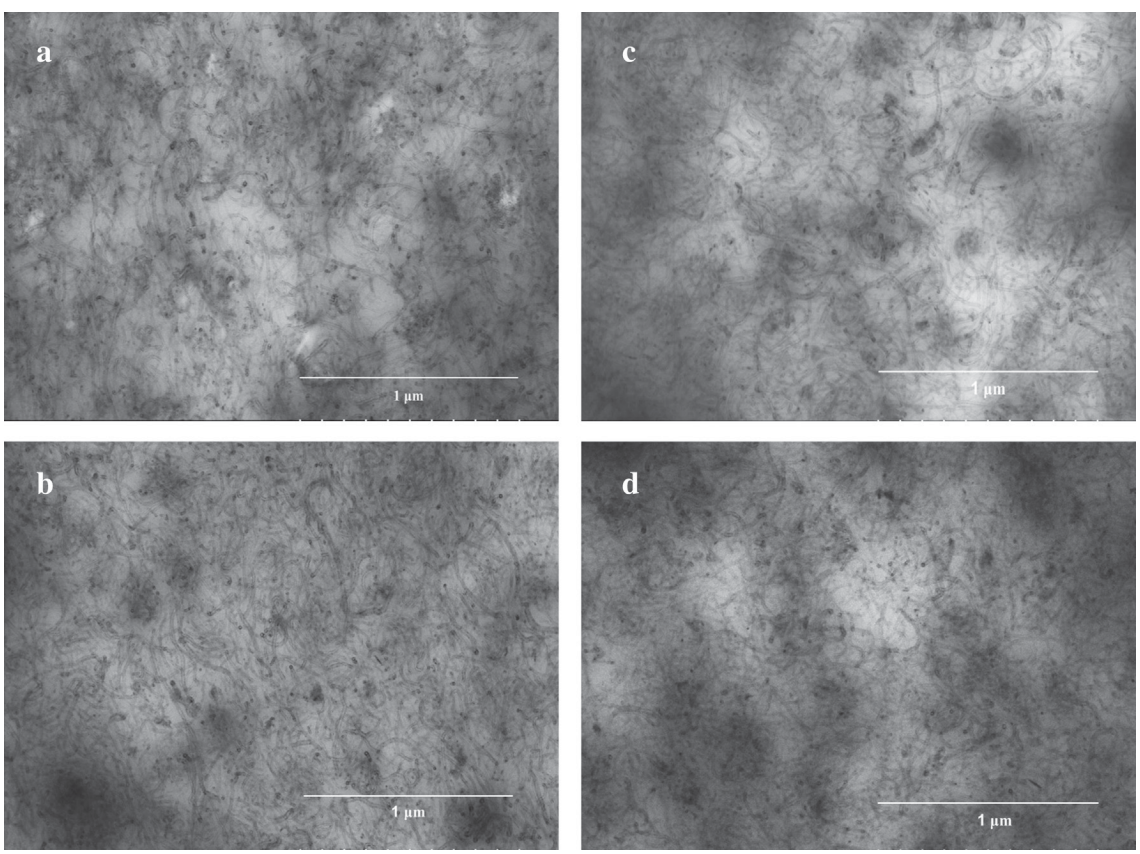

Fig. 15. STEM images for a) 15 wt.% MWCNT-SBR masterbatch as prepared, b) after mixing at 140 °C for 265 min, c) after mixing at 150 °C for 146 min, and d) after mixing at 160 °C for 97 min (Figures b–d contain 2 phr antioxidant).

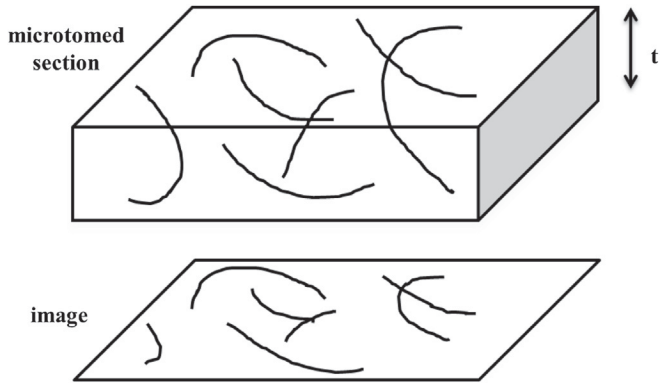

Fig. 16. Schematic representation of a microtomed STEM slice (top) and its projected image as seen by STEM (bottom).

Table 2
Contour length to end-to-end distance ratios for 25 randomly selected tubes each in the four samples from Fig. 15(a–d).

Sample name	Avg. contour length $\sum(L)/n$ (nm)	$\frac{\sum(L)}{n}/\frac{\sum(E)}{n}$	$\sum\left(\frac{L}{E}\right)/n$
MB @ 0 min/RT	324.9	1.26	1.30
MB @ 265 min/140 °C	321.1	1.43	1.90
MB @ 146 min/150 °C	341.1	1.32	1.62
MB @ 97 min/160 °C	342.8	1.38	1.74

MWCNT are well dispersed in the original masterbatch. Most MWCNTs seen in these images are not straight but are somewhat curved. The images Fig. 15b–d show the structure of the masterbatch after extensive melt processing at three temperatures and up to a maximum shear of 95.3 s^{-1}. These micrographs confirm that these oxidized MWCNTs are well dispersed in the SBR matrix with no visible signs of agglomeration or length attrition in the as-prepared masterbatch, or after melt mixing at 140 °C for 265 min, 150 °C for 146 min, or 160 °C for 97 min. This is in contrast to the reports of rearrangements to agglomerated clusters after mixing that has been reported in the literature for MWCNT in some polymer matrices [5,44–46].

It is recognized that microtome slicing to 60 nm thickness will cut some of the tubes. STEM micrographs represent a 2-dimensional (2D) view of a 3-dimensional system (3D). This is schematically illustrated in Fig. 16, where the top position is meant to represent a 3-D view of a ~50–60 nm microtomed section while the lower portion shows the resulting 2D STEM image of the former. In SBR-MWCNT composites; some tubes will be cut during the microtoming process while tubes aligned diagonally in the thickness direction will appear shorter in the 2D projection.

These artifacts of microtoming and STEM imaging must be kept in mind when attempting quantitative analysis of carbon tube lengths. ImageJ technical software was employed to measure the length of individual tubes along its surface, i.e., the contour length, and its end-to-end distance, i.e., the shortest distance between the two ends of the same tube. Analyses were performed for 25 random tubes picked from each of four STEM images (Fig. 15a–d). In Table 2 are shown the average contour lengths and two statistical analyses for measures of curvature for the 15 wt.% MWCNT masterbatch under varying mixing conditions. If the tubes were perfectly straight, as if they were rigid rods, the L/E ratio would be unity; values larger than unity are a measure of tube curvature. The average L/E ratio can be calculated two ways; one is to average L and E separately and take the ratio while another is to average the value of L/E for each tube. Table 2 shows values obtained by both methods. The L/E ratios for the as-prepared masterbatch with no additional mixing are quite similar for the two statistical methods at about 1.3.

The duration of mixing did not cause attrition of the tube contour length. It is clear that compared to the as-prepared masterbatch, there is an increase in tube curvature with mixing. It is useful to see plots of contour length versus end-to-end lengths for the 25 tubes examined for the original masterbatch (15 wt.% MWCNT) and the same masterbatch after mixing at 160 °C for 97 min, see Fig. 17a and b, since this gives some sense of the distribution of the L/E ratio as well as the absolute value of L and E. In these figures, the diagonal line represents perfectly straight tubes where the contour length and end-to-end lengths are equal; points below this line indicate the degree of curvature of the particular tube. As seen in Fig. 17a, there are more points close to the diagonal line indicating their relative straightness as compared to Fig. 17b.

3.4. STEM analysis of composites formed by dilution of 12.3 wt.% MWCNT masterbatch

Transmission electron micrographs for the uncured 12.3 wt.% MWCNT masterbatch and three diluted composites (2, 4, 7.5 wt.%

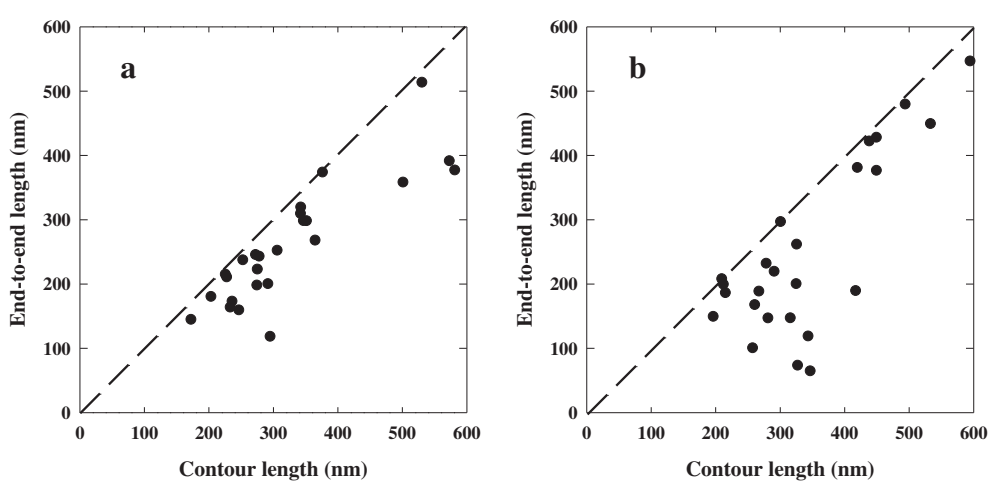

Fig. 17. Contour length (L) and end-to-end (E) distance distributions for 25 random tubes for a) as prepared 15 wt.% MWCNT masterbatch and b) masterbatch mixed at 160 °C for 97 min.

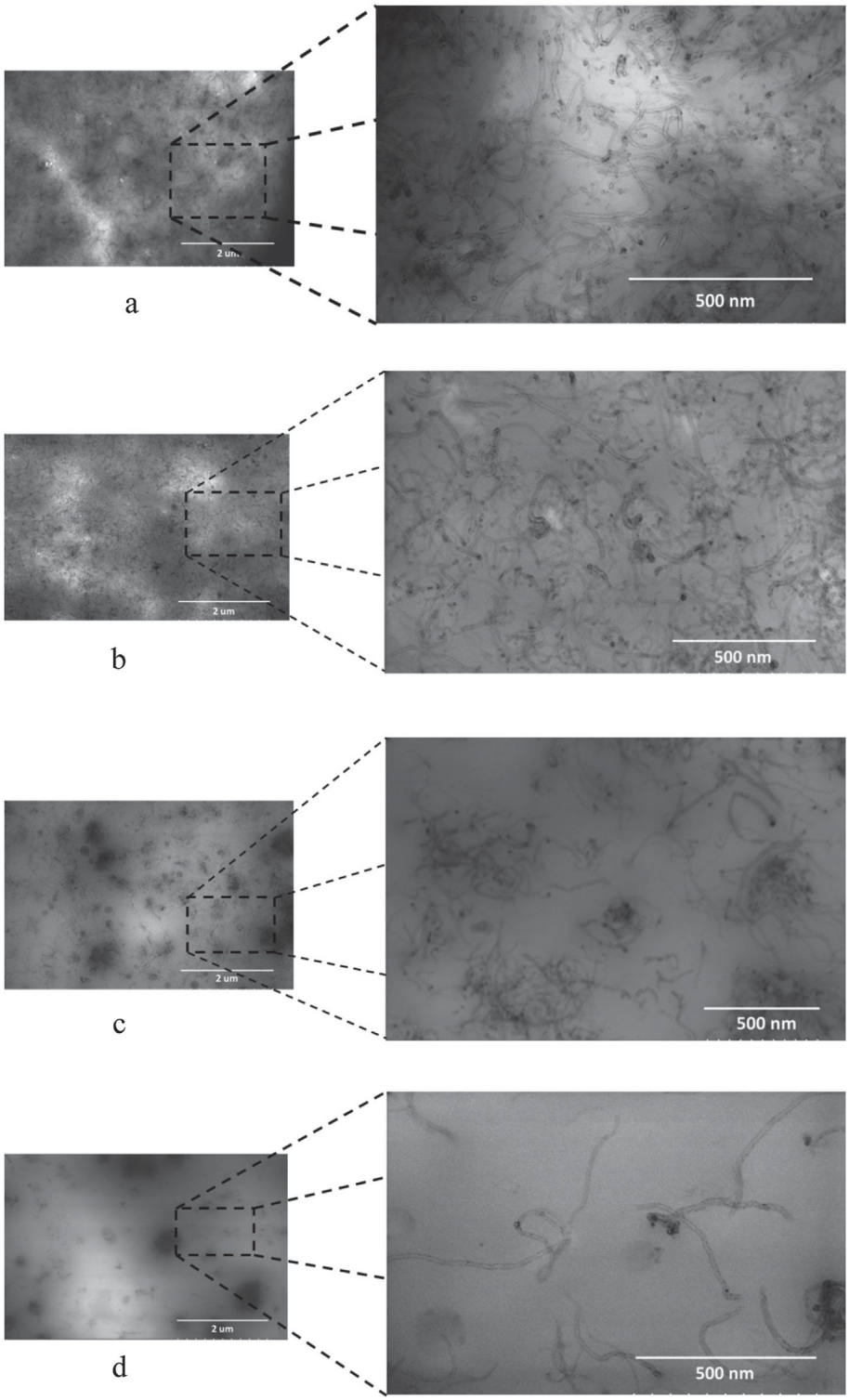

Fig. 18. Low (left) and high (right) magnification STEM images for a) original 12.3 wt.% MWCNT-SBR composite, b) 7.5 wt.%, c) 4 wt.%, and d) 2 wt.% MWCNT-SBR composites. (Note: the composites shown here are not cured).

MWCNT loadings) are shown in Fig. 18a–d respectively. In each of these figures, the left image was taken at low magnification whereas the right image was taken at a higher magnification to show the details more clearly. The dark and bright portions of these images reflect the variations in the thickness of the microtomed sections that are difficult to avoid in such materials. Fig. 18a illustrates the nature of the MWCNT dispersion for the 12.3 wt.% MWCNT masterbatch, it can be seen that the tubes are well dispersed even at high loadings of MWCNT. The higher magnification image on the right confirms that MWCNTs are well distributed in the SBR matrix without any agglomeration. However, the majority of the tubes are curved and many "C" shaped structures

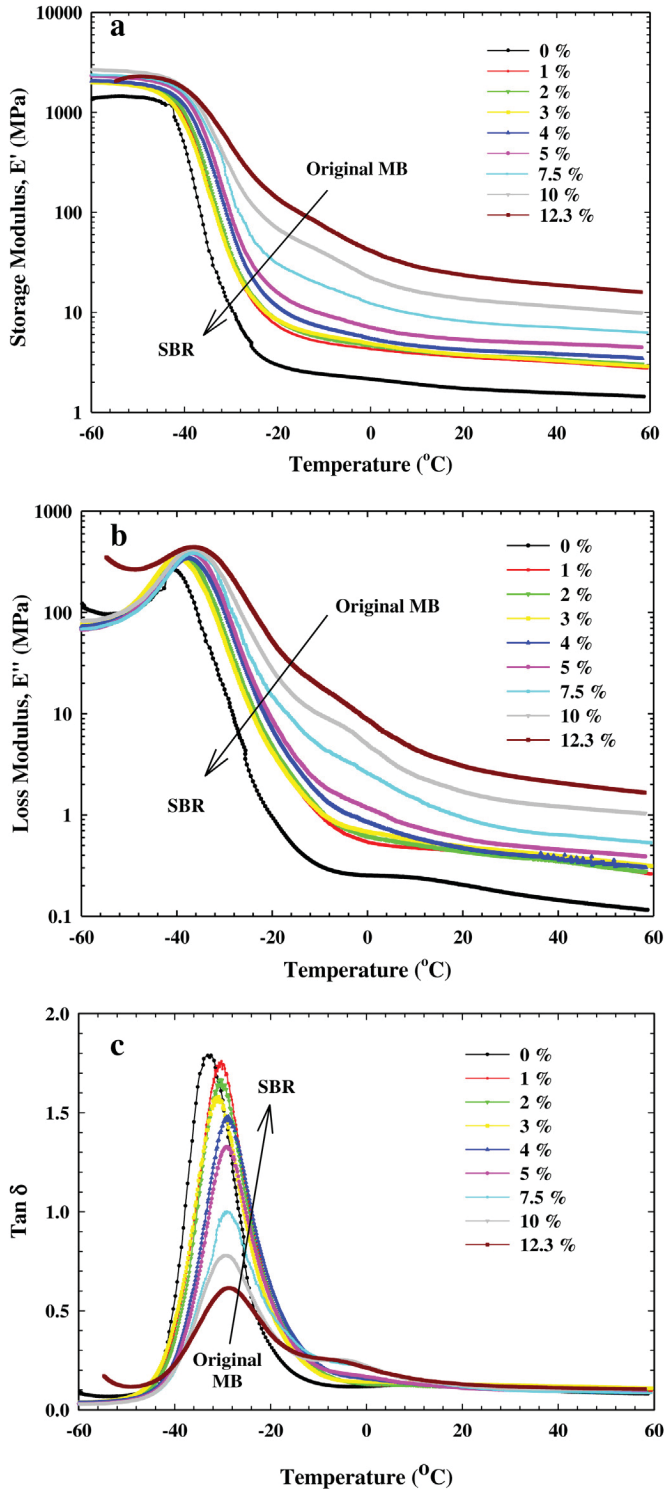

Fig. 19. Plots of a) storage modulus (E′), b) loss modulus (E″), and c) tan δ vs. temperature from DMTA for the original masterbatch (12.3 wt.% MWCNT-SBR) and various dilutions with SBR. The weight % of MWCNT in each composition is shown. (Note: For convenience, the control SBR sample with no surfactant or MWCNT was prepared by the process described in the experimental section and is labeled as 0%).

are observed. In a roller-rotor type mixer the tip of the roller at the wall of the mixing chamber forms a rolling bank of polymer fluid. This suggests that the tubes are easily conforming to the flow fields of the polymer melt.

With dilution from 12.3 wt.% MWCNT to 7.5 wt.%, see Fig. 18b, and further to 4 and 2 wt.% MWCNT loadings, Fig. 18c and d, respectively, it is seen that tubes are well separated and in the case of dilution to 2 wt.% MWCNT tubes are well dispersed. In contrast to the 2 wt.% MWCNT, the 4 wt.% MWCNT is seen to consist of a percolated network of tubes. From these micrographs, the percolation network formation (or network destruction if we are discussing in the direction of dilution) occurs between 4 and 5 wt.% MWCNT loadings which is consistent with our rheological experiments. The decreasing curvature of the tubes as seen at 2% MWCNT is consistent with the increase in the calculated aspect ratio with increased dilution shown in Table 1.

3.5. Dynamic mechanical thermal analysis (DMTA)

For the cured 12.3 wt.% MWCNT masterbatch and the various dilutions with SBR, dynamic mechanical properties were measured using a TA Q800 DMTA instrument from −60 to 60 °C at 2 °C/min under 1 Hz in tensile mode. Fig. 19a, b and c shows the storage modulus (E'), loss modulus (E'') and tan δ (E''/E') for each material versus temperature. The arrow in these figures shows the direction of dilution of the masterbatch before curing. A summary of the DMTA results is given in Table 3.

Fig. 19a shows that E′ gradually increases as the MWCNT content increases; the extent of this increase is greatest above the T_g of SBR as seen in the temperature range −20– to 60 °C due to the reinforcing effect of MWCNTs on the soft matrix. Fig. 19(b) shows E″ versus temperature; beyond the SBR T_g, E″ increases as the amount of MWCNT in the composite increases. As shown in Fig. 19b, the maximum in the E″ peak moves from −42.2 °C to −37.7 °C for the 12.3 wt.% MWCNT-SBR original masterbatch (with some ±0.5 °C fluctuations for 2, 3 and 4 wt.% diluted masterbatches). The shift in tan δ peak temperature from −33.9 °C for the cured SBR matrix to −29.5 °C for the cured 12.3% wt. MWCNT masterbatch as shown in Fig. 19c. The overall shift in E″ and tan δ peaks (the latter corresponds to the T_g of the SBR matrix) to higher temperature with increase in MWCNT loading also indicates the loss of segmental mobility of SBR and possibly due to the formation of bound rubber layer on the MWCNT surface. The increase in the tan δ peak in Fig. 19c with increasing MWCNT content is due to increased interfacial interactions between the filler and rubber. In all three curves, there seems to be a peak or shoulder between −20 °C and 5 °C; this may be attributed to the secondary network formation in the bound rubber to the MWCNT surface compared to the primary network in the SBR away from the MWCNT surface such a secondary relaxation process has been seen at 80 °C in composites of SBR with butyl rubber (BR) blends filled with 3 phr MWCNT in the presence of an ionic liquid [32]. Table 3 summarizes results from the DMTA data including effective aspect ratios for the cured original MB were calculated from the Guth–Gold–Smallwood equation for complex mechanical modulus as shown in Equation (7).

$$E_c^* = E_0^*\left(1 + 0.67\alpha\Phi + 1.62\alpha^2\Phi^2\right) \quad (7)$$

where, E_c^* and E_0^* are complex modulus of cured masterbatch and SBR matrix; and α and Φ are the effective aspect ratio and volume fraction of MWCNT loading in the composites.

The calculated aspect ratios determined in a tensile mode follow the same increasing trend with dilution of the masterbatch as the previously determined calculated aspect ratios from rheology measurements, but are about 3 times higher. This disparity probably reflects the different deformation modes involved in the two experiments, different frequencies, cured vs. uncured conditions

Table 3
Complex modulus $|E^*|$, E″ and tan δ peak temperatures and effective aspect ratios for the original MB with its diluted MBs measured at 25 °C.

Volume fraction of MWCNT, Φ	$\|E^*\|$[a] at 25 °C	E″ peak temp [°C]	tan δ peak temp [°C]	Relative E_c/E_o at 25 °C	Calculated aspect ratio, α at 25 °C
0	1.7	−42.2	−33.9	1.0	–
0.006	3.5	−40.7	−31.2	2.1	109.9
0.012	3.7	−39.5	−31.2	2.2	59.0
0.017	3.7	−40.7	−32.0	2.2	38.8
0.023	4.1	−38.0	−29.5	2.4	32.4
0.029	5.2	−38.0	−29.9	3.1	32.3
0.045	7.8	−37.9	−29.8	4.7	29.4
0.06	13.3	−37.3	−30.0	7.9	31.1
0.077	22.3	−37.7	−29.5	13.3	33.0

[a] $|E^*| = \sqrt{(E'^2) + (E''^2)}$ at 1 Hz.

and also the approximate nature of the theories. In our rheological measurements, uncured samples were mixed at 140 °C at 20 RPM (23.8 s^{-1}) whereas DMTA measurements were made on cured samples that were tested in a tensile mode from −60 to 60 °C at the temperature ramp of 2 °C/min at a frequency of 1 Hz under a sinusoidal load. The rheological measurements were made in the non-Newtonian regime of the SBR matrix at very high shear (23.8 s^{-1}); whereas, in the case of DMTA measurements, cured samples were tested at a low frequency (1 Hz) and small strain (0.01%). The latter test may only detect any smaller spheres of influence of tubes and its surroundings hence the higher aspect ratios compared with values obtained from the rheological measurements. We could consider that after curing the MWCNT is bonded to the rubber and so has greater influence on the deformation of the rubber phase surrounding the tube.

The calculated aspect ratios, α, from the rheology and DMTA measurements are shown as a function of wt.% MWCNT loading in Fig. 20. The calculated aspect ratios deduced from the DMTA data are always larger than those from the rheological data as noted earlier; however, both show a steady increase in the values of α below about 4 wt.% MWCNT. This is consistent with the physical picture described earlier.

3.6. Electrical resistivity measurements

Electrical resistivity measurements were performed on the composites obtained by dilution of the masterbatch containing 12.3 wt.% MWCNT using the experimental setup described earlier. Electrical resistivity values are plotted versus vol.% MWCNT loading in Fig. 21. As expected, resistivity decreases with increased content of MWCNT; however, the conductivity is not much affected by the presence of only 1 wt.% MWCNT loading. After this the resistivity decreases gradually at first but then more precipitously as the original masterbatch composition is reached. It is significant to note that the decrease in resistivity from neat SBR to a loading of 7.7 vol.% MWCNT, i.e., the original masterbatch, is only about two orders of magnitude. This change is much less than expected from a percolation network of conductors demonstrated repeatedly in the literature [3,34,44,47–52]. The decrease in resistivity observed can be attributed to the formation of tube–tube connections and/or electron hopping mechanisms when tubes are not actually touching each other but close enough for electron hopping [3,4]. The fact that the resistivity values for SBR and the concentrated masterbatch is only two orders different suggests that the MWCNTs are dispersed as individual tubes and are well covered with SBR matrix as seen by STEM.

4. Summary

Surface modified MWCNT-SBR masterbatches with up to 15 wt.% MWCNT were prepared by a cost effective coagulation process followed by melt mastication in a lab scale Haake batch mixer simulating the mixing profile in the industrial Banbury batch mixer. STEM images of these masterbatches reveal that the MWCNTs at 15 wt.% are uniformly well dispersed. Analysis of the contour length and the end-to-end lengths of tubes obtained from STEM images showed no attrition of contour length and increasing curvature of tubes with increasing shear mixing.

On melt dilution of the masterbatch containing 12.3 wt.% MWCNT with the same SBR as the matrix, changes in melt viscosity response were observed in the MWCNT concentration range 2.6–4.0 wt.%. STEM images of these uncured blends confirm that the MWCNTs in the original masterbatch contain many closely packed and overlapping curved tubes which transform into well-separated tubes (as seen in 2 wt.% MWCNT-SBR composite) with dilution. The transition from overlapping to non-overlapping and straighter tubes is seen around 4 wt.% MWCNT (~2.5 vol.% MWCNT) loading. The calculated aspect ratios of the masterbatch and dilutions from

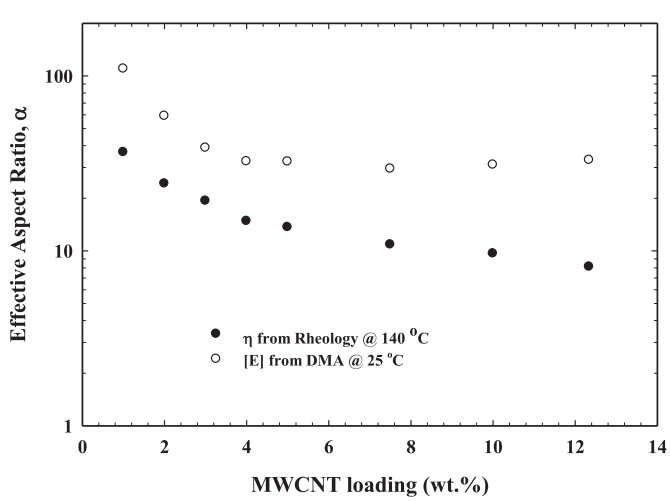

Fig. 20. Comparison of calculated aspect ratios calculated from rheology at 140 °C and DMTA at 25 °C.

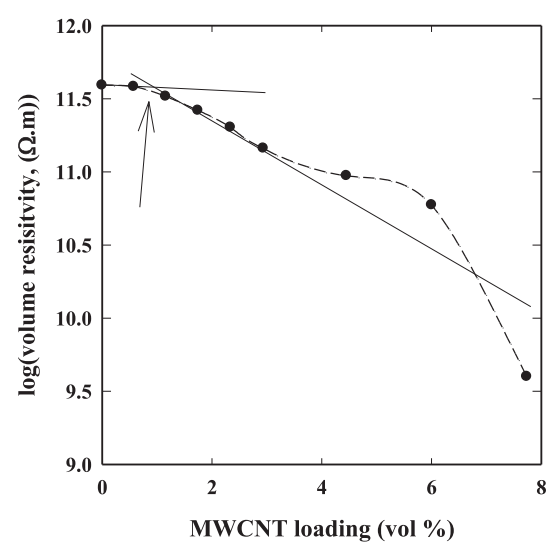

Fig. 21. Volume resistivity versus volume fraction of MWCNT obtained by dilutions of the 12.3 wt.% MWCNT-SBR MB with SBR.

the rheology data using the Guth–Gold–Smallwood equation followed the same trend as seen by their morphologies, increasing with increasing dilution of the MWCNT.

The T_g of cured plaques by DMTA was shown to increase 4.5 °C with dilution of the SBR masterbatch containing 12.3 wt.% MWCNT. The formation of a rubber layer bound to the MWCNT was characterized by the onset of a shoulder from −5– to 20 °C in E′, E″ and tan δ vs. temperature plots. As with the melt rheology, the calculated aspect ratios reflect the trend of tube morphology, although the calculated values from DMTA for cured composites are larger than from the rheology of uncured composites. Bulk electrical resistivity measurements of the masterbatch and its dilutions indicate that the tubes are well separated within the matrix. A transition in resistivity is also observed around 2 vol.% MWCNT.

The flexibility of the MWCNT when dispersed as discrete tubes is quite remarkable. The tubes are observed to conform readily to the flow fields generated during melt mixing. It is clear that the use of the tube aspect ratio from simple considerations of their contour length and diameter are inadequate to predict their rheological and mechanical performance. Factors must be considered such as the degree of individual tube dispersion, tube conformational changes, and their degree of bonding to the matrix.

Acknowledgments

The authors would like to thank Dr. M.F. Finlayson for preparing the masterbatch and also like to thank Molecular Rebar Design, LLC for funding this project and instrumentation support. J. Kiesekamp, S. Ilisch and D. Bellgardt, Styron Europe GmbH, are thanked for their helpful discussions.

References

[1] Iijima S. Nature 1991;354(6348):56–8.
[2] Pötschke P, Fornes TD, Paul DR. Polymer 2002;43(11):3247–55.
[3] Hu GJ, Zhao CG, Zhang SM, Yang MS, Wang ZG. Polymer 2006;47(1):480–8.
[4] McNally T, Pötschke P, Halley P, Murphy M, Martin D, Bell SEJ, et al. Polymer 2005;46(19):8222–32.
[5] Pötschke P, Abdel-Goad M, Alig I, Dudkin S, Lellinger D. Polymer 2004;45(26):8863–70.
[6] Lin B, Sundararaj U, Pötschke P. Macromol Mater Eng 2006;291(3):227–38.
[7] Moniruzzaman M, Winey KI. Macromolecules 2006;39(16):5194–205.
[8] Du JH, Bai J, Cheng HM. Express Polym Lett 2007;1(5):253–73.
[9] Bokobza L. Polymer 2007;48(17):4907–20.
[10] Bhattacharya M, Maiti M, Bhowmick AK. Polym Eng Sci 2009;49(1):81–98.
[11] Sengupta R, Ganguly A, Sabharwal S, Chaki TK, Bhowmick AK. J Mater Sci 2007;42(3):923–34.
[12] Thess A, Lee R, Nikolaev P, Dai HJ, Petit P, Robert J, et al. Science 1996;273(5274):483–7.
[13] Skipa T, Lellinger D, Boehm W, Saphiannikova M, Alig I. Polymer 2010;51(1):201–10.
[14] Charlier JC. Acc Chem Res 2002;35(12):1063–9.
[15] Halpin JC. J Compos Mater 1969;3:732.
[16] Gojny FH, Schulte K. Compos Sci Technol 2004;64(15):2303–8.
[17] Ramanathan T, Liu H, Brinson LC. J Polym Sci Part B Polym Phys 2005;43(17):2269–79.
[18] Wu HL, Yang YY, Ma CCM, Kuan HC. J Polym Sci Part A Polym Chem 2005;43(23):6084–94.
[19] Barraza HJ, Pompeo F, O'Rear EA, Resasco DE. Nano Lett 2002;2(8):797–802.
[20] Yu YJ, Chu OY, Gao Y, Si ZH, Chen W, Wang ZQ, et al. J Polym Sci Part A Polym Chem 2005;43(23):6105–15.
[21] Ham HT, Choi YS, Chee MG, Chung IJ. J Polym Sci Part A Polym Chem 2006;44(1):573–84.
[22] Kwon J, Kim H. J Polym Sci Part A Polym Chem 2005;43(17):3973–85.
[23] Xie HF, Liu BH, Yuan ZR, Shen JY, Cheng RS. J Polym Sci Part B Polym Phys 2004;42(20):3701–12.
[24] Du FM, Fischer JE, Winey KI. J Polym Sci Part B Polym Phys 2003;41(24):3333–8.
[25] Dondero WE, Gorga RE. J Polym Sci Part B Polym Phys 2006;44(5):864–78.
[26] Gorga RE, Cohen RE. J Polym Sci Part B Polym Phys 2004;42(14):2690–702.
[27] Kim JY, Kim SH. J Polym Sci Part B Polym Phys 2006;44(7):1062–71.
[28] Pham JQ, Mitchell CA, Bahr JL, Tour JM, Krishanamoorti R, Green PF. J Polym Sci Part B Polym Phys 2003;41(24):3339–45.
[29] Gong XY, Liu J, Baskaran S, Voise RD, Young JS. Chem Mater 2000;12(4):1049–52.
[30] Datsyuk V, Kalyva M, Papagelis K, Parthenios J, Tasis D, Siokou A, et al. Carbon 2008;46(6):833–40.
[31] Treacy MMJ, Ebbesen TW, Gibson JM. Nature 1996;381(6584):678–80.
[32] Wu D, Wu L, Zhou W, Sun Y, Zhang M. J Polym Sci Part B Polym Phys 2010;48(4):479–89.
[33] Global tires & rubber report. Marketline Pub; May 2012.
[34] Abdel-Goad M, Pötschke P. J Non-Newton Fluid 2005;128(1):2–6.
[35] Pötschke P, Bhattacharyya AR, Janke A, Goering H. Adv Polycarbonates 2005:148–63.
[36] Handge UA, Pötschke P. Rheol Acta 2007;46(6):889–98.
[37] Bruhwiler PA, Barbezat M, Necola A, Kohls DJ, Bunk O, Schaefer DW, et al. J Mater Res 2010;25(6):1118–30.
[38] Goodrich JE, Porter RS. Polym Eng Sci 1967;7:45–51.
[39] Bousmina M, Ait-Kadi A, Faisant JB. J Rheol 1999;43(2):415–33.
[40] Wang J, James DF, Park CB. J Rheol 2010;54(1):95–116.
[41] Guth E. J Appl Phys 1945;16(1):20–5.
[42] Smallwood HM. J Appl Phys 1944;15(11):758–66.
[43] Guth E, Gold O. Phys Rev 1938;53:322.
[44] Alig I, Skipa T, Lellinger D, Pötschke P. Polymer 2008;49(16):3524–32.
[45] Alig I, Lellinger D, Engel M, Skipa T, Pötschke P. Polymer 2008;49(7):1902–9.
[46] Pötschke P, Bhattacharyya AR, Alig I, Dudkin SM, Leonhardt A, Taschner C, et al. In: Kuzmany H, Fink J, Mehring M, Roth S, editors. Electronic properties of synthetic nanostructures 2004. pp. 478–82.
[47] Das A, Stöckelhuber KW, Jurk R, Fritzsche J, Klüppel M, Heinrich G. Carbon 2009;47(14):3313–21.
[48] Weber M, Kamal MR. Polym Compos 1997;18(6):711–25.
[49] Micusik M, Omastova M, Krupa I, Prokes J, Pissis P, Logakis E, et al. J Appl Polym Sci 2009;113(4):2536–51.
[50] Logakis E, Pissis P, Pospiech D, Korwitz A, Krause B, Reuter U, et al. Eur Polym J 2010;46(5):928–36.
[51] Hombostel B, Pötschke P, Kotz J, Roth S. Phys Status Solidi B 2006;243(13):3445–51.
[52] Hombostel B, Dubosc M, Pötschke P, Roth S. In: Kuzmany H, Fink J, Mehring M, Roth S, editors. Electronic properties of synthetic nanostructures 2004. p. 473.